Microstructure control of cold-sprayed pure iron coatings formed using mechanically milled powder

doi: 10.1016/j.surfcoat.2018.10.016

Elsevier Editorial System(tm) for Surface and Coatings Technology

Manuscript Draft

Manuscript Number: SURFCOAT-D-18-01040R2

Title: Microstructure control of cold-sprayed pure iron coatings formed using mechanically milled powder

Article Type: Full Length Article

Keywords: Cold spraying; Mechanical milling; Nanocrystalline material; Pure iron; Microstructre; Electron backscatter diffraction

Corresponding Author: Dr. Kiyohiro Ito, Assistant Professor

Corresponding Author's Institution: Tokyo University of Science

First Author: Kiyohiro Ito, Assistant Professor

Order of Authors: Kiyohiro Ito, Assistant Professor; Yuji Ichikawa, Assistant Professor

Abstract: Nanocrystalline metallic materials with grain sizes of less than 100 nm exhibit high strength and unique characteristics, such as high levels of ductility and corrosion resistance. Mechanical milling techniques can be used to produce large amounts of nanocrystalline metallic powder. However, it is essential to perform a sintering treatment, which induces coarsening of the crystal grains, to form a bulk material from the mechanically milled powder. The cold spray technique is expected to effectively form a nanocrystalline metallic coating using the mechanically milled powder. This study focuses on pure iron coating, which is formed by a cold spray technique using mechanically milled pure iron powder. Pure iron powder, with crystal grains of ~100 nm, was obtained by a mechanical milling process, and was deposited onto a low-carbon steel substrate by cold spraying. It was confirmed that a dense, nanocrystalline coating with a hardness of over 300 HV can be achieved; however, the deposition efficiency of this coating was half of that of the coating formed using the as-received powder. The improvement of the deposition efficiency and properties of such coatings was attempted using powder mixtures comprising both milled and as-received powders. The results indicate that the deposition efficiency and microstructure, directly linked to the mechanical properties of the coating, can be controlled by varying the content of the as-received powder of the mixture.

Highlights

- The nanocrystalline pure iron coating can be obtained by employing mechanical milling combined with cold spraying.
- The deposition efficiency and microstructure can be controlled using powder mixtures comprising both milled and as-received powders.
- The milled and as-received powders in the mixture are deposited on the substrate independently without interaction with each other.

Microstructure control of cold-sprayed pure iron coatings formed using mechanically milled powder

Kiyohiro Ito[1] and Yuji Ichikawa[2]

1. Department of Mechanical Engineering, Tokyo University of Science, 6-3-1, Niijuku, Katsushika-ku, Tokyo 125-8585, Japan

E-mail address: kiyohiro@rs.tus.ac.jp

2. Fracture and Reliability Research Institute, Tohoku University, Aoba 6-6-11-703, Aramaki, Aoba-ku, Sendai 980-8579, Japan

E-mail address: ichikawa@rift.mech.tohoku.ac.jp

Abstract

Nanocrystalline metallic materials with grain sizes of less than 100 nm exhibit high strength and unique characteristics, such as high levels of ductility and corrosion resistance. Mechanical milling techniques can be used to produce large amounts of nanocrystalline metallic powder. However, it is essential to perform a sintering treatment, which induces coarsening of the crystal grains, to form a bulk material from the mechanically milled powder. The cold spray technique is expected to effectively form a nanocrystalline metallic coating using the mechanically milled powder. This study focuses on pure iron coating, which is formed by a cold spray technique using mechanically milled pure iron powder. Pure iron powder, with crystal grains of ~100 nm, was obtained by a mechanical milling process, and was deposited onto a low-carbon steel substrate by cold spraying. It was confirmed that a dense, nanocrystalline coating with a hardness of over 300 HV can be achieved; however, the deposition efficiency of this coating was half of that of the coating formed using the as-received powder. The improvement of the deposition efficiency and properties of such coatings was attempted using powder mixtures comprising both milled and as-received

powders. The results indicate that the deposition efficiency and microstructure, directly linked to the mechanical properties of the coating, can be controlled by varying the content of the as-received powder of the mixture.

Keywords

Cold spraying, Mechanical milling, Nanocrystalline material, Pure iron, Microstructure, Electron backscatter diffraction

*Corresponding author: Tel.: +81-3-5876-1823, Fax: +81-3-5876-1823

E-mail address: kiyohiro@rs.tus.ac.jp (Kiyohiro Ito)

1. Introduction

In power and chemical plants, high chromium steels or stainless steels, which exhibit high strength and high corrosion resistance, are employed for components, such as pipes and turbine blades. Typically, these excellent properties are achieved by adding rare metals or strategic materials to the base metal. However, for the effective utilization of resources, the improvement of these properties without the use of rare metals or strategic materials is desirable.

Grain refinement is a technique used for the reinforcement of metallic materials without the addition of rare metals or strategic materials. In particular, nanocrystalline metallic materials, which are generally defined as materials with grain sizes smaller than 100 nm, have high strengths exceeding those of coarse-grained and even alloyed metallic materials [1]. Furthermore, nanocrystalline metallic materials can exhibit high levels of ductility and corrosion resistance [2–4]. These unique characteristics have attracted the attention of several researchers. A number of techniques have been proposed to achieve nanocrystallization of metallic materials, such as thermo-mechanical-controlled processes, equal-channel angular pressing, accumulative roll-bonding, and mechanical-milling [5–8]. These techniques are based on the introduction of severe plastic strain to metallic materials and dynamic recrystallization. Among these techniques, mechanical milling can be used to produce large quantities of nanocrystalline metallic powders relatively conveniently. During the mechanical milling process, the powder material is repeatedly deformed by the high-energy impact of the balls. However, it is essential to conduct a sintering treatment at high temperature to form a bulk material from the nanocrystallized powder produced by the mechanical milling process. High-temperature treatments induce coarsening of the nanocrystal grains obtained by the mechanical milling process.

Cold spray techniques are based on the impact and deposition of numerous fine and

solid particles accelerated by a supersonic gas flow [9,10]. Such cold spray processes are performed below the melting temperature of the powder material; thus, they are capable of maintaining the microstructure of the feedstock powder. This suggests that nanocrystalline metallic coatings can easily be achieved by the application of mechanical milling, combined with cold spraying. A number of nanocrystalline coatings, such as aluminum alloys, copper alloys, nickel alloys, and intermetallic alloys, formed by cold spraying using mechanically milled powder, have previously been investigated [11–16]. Ajdelsztajn et al. reported that an Al 5083 powder with nanocrystalline grains in the range of 20–30 nm can be obtained by performing mechanical milling under a liquid nitrogen environment. In addition, it has been confirmed that nanocrystalline Al 5083 coatings can be formed by cold spraying; the hardness values of these coatings are significantly higher than those of cast or cold worked Al 5083 [17]. Kumar et al. confirmed the successful formulation and deposition of nanocrystalline Ni–20Cr powder, with an average crystal grain-size of 10 nm, onto SA 516 boiler steel by a cold spray technique [18,19]. The nanocrystalline Ni–20Cr coating provided superior high-temperature oxidation resistance and erosion–corrosion resistance compared to those of boiler steel and coarse-grained Ni–20Cr coatings.

As shown by these reports, nanocrystalline metallic coatings can be obtained by employing mechanical milling combined with cold spraying. This study focuses on a pure iron coating, formed by cold spraying using mechanically milled feedstock powder, as an alternative material to high chromium or stainless steels. Commercially available pure iron powder was mechanically milled under various conditions, and characterized to determine the optimal milling conditions. The powder was milled under specific conditions, and then, it was deposited onto a low-carbon steel substrate by cold spraying. The deposition efficiency, microstructure, and hardness of the obtained coating were evaluated using scanning electron microscopy (SEM), electron backscatter diffraction (EBSD) analysis, and hardness testing.

2 Experimental procedures

2.1 Mechanical milling conditions

A commercially available pure iron powder (ITOH KIKOH CO., LTD., Japan) was employed as the feedstock powder for the cold spray process. The chemical composition of the iron powder, shown in Table I, was identified using an optical emission spectrometer (PDA-5500, Shimadzu Corporation, Japan) and a carbon and sulfur analyzer (EMIA-220V, HORIBA, Ltd., Japan). The pure iron powder was treated by using a commercial planetary ball milling equipment (Planetary Micro Mill PULVERISETTE 7, Fritsch Co., Ltd, Germany). The iron powder was placed in a silicon-nitride pod, with an inner volume of 45 mL, together with high-carbon chromium bearing steel balls (JIS code: SUJ2, Ohashikokyu Co., Ltd., Japan). The diameter of each SUJ2 ball was 8 mm and the masses of the iron powder and the balls were approximately 50 g and 73 g, respectively. The rotation speed of the pod was constant at 1400 rpm. The total milling periods were set to 5 h, 10 h, and 20 h. Cycles including a milling period of 30 min, followed by a rest period of 15 min, were repeated throughout the total milling period. The mechanical milling process was performed under an air atmosphere. The particle size distributions of the as-received and milled powders were identified by a laser diffraction and scattering method (Microtrac MT3300EX II, Nikkiso Co., Ltd., Japan). In this study, the mean particle size was equivalent to that where the cumulative volume of the powder was 50% of the total volume of the powder.

2.2 Cold spraying conditions

The as-received and mechanically milled iron powders were deposited onto a low-carbon steel substrate (JIS code: SS400) using a high-pressure cold spray technique. A commercial cold spray facility (PCS-100, Plasma Giken Co., Ltd., Japan) was used. Nitrogen

gas was used as the acceleration and carrier gases for the iron powder. The pressure and temperature of the acceleration gas were maintained as 5 MPa and 1273 K, respectively. The rotational speed of the powder feeder, which is associated with the powder feed rate, was 3 rpm and the traverse speed of the spray gun nozzle was 300 mm/s. The standoff distance between the spray gun nozzle tip and the substrate was maintained at 30 mm.

2.3 Deposition efficiency

The deposition efficiencies of the as-received and mechanically milled iron powders were evaluated based on the weight ratio between the deposited powder and consumed powder. The deposition efficiency η is given as

$$\eta = \frac{W_{deposited}}{W_{consumed}} \times 100\ [\%]\ , \tag{1}$$

where $W_{deposited}$ and $W_{consumed}$ represent the weights of the deposited powder and consumed powder, respectively. In addition, 100 g of each powder was placed into the powder feeder and sprayed onto the substrate. The value of $W_{deposited}$ was obtained by subtracting the weight of the substrate measured prior to the spraying from that measured following the spraying.

2.4 Observation of microstructure

The microstructures of the cold-sprayed iron coatings were observed using SEM. In addition, EBSD analysis was used to study the crystal grain-size distribution of the coating. The iron coatings were cut perpendicular to the coating surface, and embedded in epoxy resin (Epoxicure 2, Buehler, USA). The cross-sectional surfaces of the coatings were successively ground with #80, #320, and #600 waterproof abrasive papers, and polished with diamond suspensions of 9 μm, 3 μm, and 1 μm. Subsequently, the cross-sectional surfaces were

mirror-polished with 0.05 μm colloidal silica (Mastermet, Buehler, USA). To prevent the development of the charge-up phenomenon during the SEM observation, the cross-sectional surfaces were coated with Au, using a sputtering technique (MC1000, Hitachi High-Technologies Corporation, Japan). The area designated for observation was treated for a period of 4 min using a flat ion milling technique (IM4000, Hitachi High-Technologies Corporation, Japan). For the microstructural observation a commercial field emission SEM (SU-70, Hitachi High-Technologies Corporation, Japan) was used.

The porosity of each coating was assessed by performing image analysis on the cross-sectional SEM images, using the free software ImageJ (U. S. National Institutes of Health, USA)[20]. The SEM images were magnified by ×250 and the porosity of each coating was assessed using five SEM images. In this study, splat boundaries in a coating were also regarded as pores.

The crystal grain-size distributions were investigated by EBSD analysis, using equipment manufactured by the TexSEM Laboratories, Inc., USA. During the EBSD analysis, two step sizes of 100 nm and 15 nm were employed to analyze the relatively large and small areas selected for the investigation, respectively. Any images of the crystal grains with an image quality of less than 1000 due to the problems with the detection accuracy were excluded.

2.5 Hardness tests

The hardness of each coating was measured using a micro Vickers hardness tester (MICRO-SA, Matsuzawa Co., Ltd, Japan). The specimens used for the cross-sectional observations were also used for the hardness tests. The vertical load was set to 0.98 N and the hardness of each coating was randomly measured 15 times. The mean value of the measurements was recorded as the hardness of the coating.

3. Results and discussion

3.1 Characterization of the milled powder

The SEM images of the as-received powder and the powders that were mechanically milled for various periods of time are shown in Fig. 1. The morphologies of the milled powders significantly differ from that of the as-received powder. The as-received powder has a spherical shape; in contrast, the milled powders have irregular and angular shapes. In addition, the qualitative inspection of the SEM images show that the particles of the milled powders are generally larger than those of the as-received powder.

The particle-size distribution of the as-received powder and the milled powders is shown in Fig. 2. The particle-size distribution of the as-received powder is relatively narrow. Nevertheless, the particle sizes of the milled powders are in the range of 5–500 μm. The maximum particle size of the milled powders was approximately ten times larger than that of the as-received powder. This indicates that the particles merged with each other during the mechanical milling process. The relationship between the mechanical milling treatment period and the mean particle size is shown in Fig. 3. The mean particle size increases as the treatment time is extended to 10 h. However, the mean particle size decreases when the treatment time is set to 20 h. There was also a decrease in the maximum particle size of the powder that was milled for 20 h, as shown in Fig. 2. These results imply that the merged particles began to fragment when the treatment period was set to 20 h. Compared with the other milled powders, the powder that was milled for 20 h has a more appropriate particle size for cold spraying.

Figure 4 shows inverse pole figure (IPF) images, obtained by EBSD analysis, of the cross-sections of the particles of the as-received powder and the powder that was milled for 20 h. The colors in the IPF images represent crystal orientations. Based on these IPF images, it was confirmed that the powder that was milled for 20 h exhibited much finer crystal grains

than the as-received powder. In addition, these fine crystal grains were distributed throughout the powder milled for 20 h. The crystal grain-size distributions of the as-received powder and the powder milled for 20 h are shown in Fig. 5. The as-received powder exhibits crystals with grain sizes larger than 1 μm. Furthermore, for the powder milled for 20 h, the mode value of the crystal grain-size is approximately 100 nm. No crystals with a grain size larger than 1 μm can be observed. In addition, several fine crystals with grain sizes smaller than 50 nm can be observed. Consequently, it is confirmed that pure iron powder can be nanocrystallized using mechanical milling techniques.

3.2 Characterization of the coating formed using the milled powder

Based on the results of the mechanical milling, the powder milled for 20 h, hereinafter referred to as the milled powder, was selected as a feedstock powder for the cold spray process. In this study, cold-sprayed coatings were formed using the as-received powder and milled powder, which are denoted by STD and MM, respectively.

Figure 6 shows the cross-sectional SEM images of the STD and MM coatings. Both the STD and MM coatings are dense, with thicknesses of more than 500 μm, as shown in Figs. 6(a) and 6(c). Further, no cracks can be observed at the coating/substrate interface. Based on the high-magnification images shown in Figs. 6(b) and 6(d), it was confirmed that the microstructure of the MM coating differs from that of the STD coating. Relatively large pores of ~10 μm, as well as crystal grains, can be observed in the image of the STD coating. In contrast, neither large pores nor crystal grains can be observed in the image of the MM coating. However, several splat boundaries can be observed, which has similar appearance to that of cracked glass. A number of these splat boundaries were formed by the collapse and bonding of particles during the mechanical milling process. As described later, the deposition efficiency of the milled powder was significantly lower than that of the as-received powder.

This indicates that a large number of particles of the milled powder containing large particles with sizes larger than 100 μm were impinged on the deposited layer without deposition. These wasted particles probably contributed to the disappearance of large pores, similarly to shot peening.

The IPF images of these two coatings, obtained by EBSD analysis, are shown in Fig. 7. In the case of the STD coating, crystal grains with sizes larger than 10 μm are widely distributed. The high-magnification image shown in Fig. 7(b) reveals the presence of crystal grains smaller than 1 μm at the particle/particle interface. These fine crystal grains could not be detected within the as-received powder. Thus, the crystal grains in the vicinity of the particle/particle interface were refined by the appearance of dynamic recrystallization at the moment of impingement or during the formation of the coating. However, these fine crystal grains do not contribute to a significant proportion of the coating. In contrast, the crystal grain-size of the MM coating was completely different from that of the STD coating. In the case of the MM coating, shown in Figs. 7(c) and 7(d), nanocrystal grains are distributed throughout the coating; crystal grains with a size larger than 1 μm cannot be observed. The crystal grain-size distributions of the STD and the MM coatings are shown in Fig. 8. Compared with the crystal grain-size of the milled powder, shown in Fig. 4(c), the crystal grains of the MM coating were slightly larger; however, nanocrystal grains were maintained. The substrate and the deposited layer were exposed to the high temperature gas stream and heated up during the cold spray process. The coarsening of the crystal grains can be attributed to the high temperature of the accelerating gas. The behavior of crystal grain growth is influenced by the plastic strain in the crystal grains. Crystal grains with large plastic strains, i.e., numerous dislocations, can be easily recrystallized and coarsened by heating. The coarsened crystal grains observed in Fig. 7(d) probably possess large plastic strains induced by the mechanical milling. On the other hand, there are few plastic strains in the fine crystal

grains. A similar crystal grain growth behavior can also be observed in cold-sprayed metallic coatings subjected to heat treatment at a relatively low temperature [21].

The hardness, deposition efficiency, and porosity of the STD and MM coatings are shown and compared in Fig. 9. The hardness of the MM coating was determined to be more than double of that of the STD coating. The higher hardness of the MM coating can be attributed to the presence of the nanocrystal grains. In contrast, the deposition efficiency of the as-received powder was determined to be approximately double of that of the milled powder. Moreover, the degree of porosity of the MM coating, which includes the splat boundaries observed in Fig. 6(d), was estimated to be approximately double of that of the STD coating. During the cold spray process, it is more difficult to plastically deform the milled powder with a high hardness, than the as-received powder. The large plastic deformation of the powder results in the elimination of the natural oxide film present on the powder surface and on the intimate contact between the powders and the substrate or deposited coating layer, followed by the deposition of the powder [22]. Specifically, a low degree of plastic deformation results in a low bonding strength between the particles, as well as a low deposition efficiency. In addition, the milled powder exhibits a wide particle-size distribution, and also contains particles with sizes larger than 100 μm, as shown in Fig. 2. It is difficult to deposit these large particles by cold spraying [23]; however, the angular shapes of the milled powder contribute to deposition compared to the spherical shapes of the as-received powder [24]. Consequently, the comparatively low deposition efficiency and high porosity level of the MM coating can be attributed to the high hardness, wide particle-size distribution, and splat boundaries of the milled powder, which were already formed during the mechanical milling process.

Based on these results, we demonstrated that a dense, pure iron coating with high hardness can be achieved using the milled powder with nanocrystal grains. Furthermore, the

deposition efficiency of the milled powder was significantly lower than that of the as-received powder. Therefore, we attempted to improve the deposition efficiency of the milled powder, which is discussed in section 3.3.

3.3 Characterization of the coating formed using a mixed powder

To improve the deposition efficiency of the milled powder, it was mixed with the as-received powder. The mixed powder was cold-sprayed onto a SS400 substrate under the conditions described in section 2.2. The mixing ratio between the as-received powder and milled powder was varied to investigate the effect of the mixing ratio on the deposition efficiency, microstructure, and hardness of the coating. Milled powder samples with as-received powder contents of 10 wt.%, 20 wt.%, and 30 wt.% were prepared, denoted as AS10, AS20, and AS30, respectively.

The cross-sectional SEM images of the coatings formed using each powder are shown in Fig. 10. Dense coatings with thicknesses larger than 500 μm can be seen in Figs. 10(a), 10(c), and 10(e). The magnified images indicate that relatively large pores and several splat boundaries are present; however, the appearance of these splat boundaries do not resemble to cracked glass. As shown in Figs. 6(b) and 6(d), the microstructures of the three coatings formed by the mixed powders were more similar to that of the STD coating than that of the MM coating.

The IPF images of the three coatings, obtained by EBSD analysis, are shown in Fig. 11. A number of regions with coarse crystal grains can be observed in the case of the AS10 coating. These regions originated from the as-received powder. In addition, the proportion of the as-received powders within the coating noticeably increases as the as-received powder content of the mixed powder increases. These results indicate that the as-received powders can be widely scattered throughout the coating that was formed using the

mixed powder. Furthermore, the degree of distribution of the as-received powders in the coating matrix can be controlled by varying the content of the as-received powder of the mixed powder. These microstructures exhibit both nanocrystal grains and coarse crystal grains. Zhang et al. reported that harmonic structures, with a bimodal grain-size distribution with a specific periodic arrangement of coarse and ultrafine grain fractions, can be used to achieve both high strength and high ductility [25]. Referring to the work reported by Zhang et al., these microstructures, shown in Fig. 11, are expected to exhibit excellent mechanical properties.

The relationship between the deposition efficiency and the content of the as-received powder of the mixed powder is shown in Fig. 12(a). The deposition efficiency linearly increases as the content of the as-received powder of the mixture increases. A deposition efficiency of approximately 45% can be obtained using the AS30 powder. Let us assume that the deposition efficiencies of the milled powder and as-received powder are maintained when the mixed powder are sprayed on the substrate. Using the deposition efficiency, η_{milled}, of the milled powder and the deposition efficiency, η_{as}, of the as-received powder, the deposition efficiency, η_{mixed}, of the mixed powder can be expressed as

$$\eta_{mixed} = \frac{(\eta_{as} - \eta_{milled})}{100} \times \xi_{as} + \eta_{milled}\ [\%]\,, \tag{2}$$

where ξ_{as} is the content of the as-received powder of the mixed powder. According to the assumption, the deposition efficiency of the mixed powder is expected to be proportional to the content of the as-received powder. Consequently, the experimental result indicates that the milled and the as-received powders are deposited on the substrate independently without interaction with each other. This means that the deposition efficiency of the milled powder itself is not improved by the mixture of the as-received powder with the milled powder.

The porosity level and Vickers hardness of each coating are shown in Figs. 12(b) and 12(c) as a function of the as-received powder content, respectively. In contrast to the deposition efficiency, the porosity level and Vickers hardness monotonically decrease as the as-received powder content of the mixture increases. The assumption above is extended to the porosity level of each coating. If the porosity of the coating is determined by sum of the porosities resulting from the milled and the as-received powders, the porosity of the coating is expected to be the black line shown in Fig. 12(b). The tendency of the experimental result is similar to the expected line. This also indicates that the depositions of the milled and the as-received powders are independent of each other.

Our previous research has revealed that the most important factor in the deposition of cold-sprayed metallic particles on a metallic substrate is a natural oxide film on the particles and the substrate [22][26]. The milled and as-received powders are obviously composed of the same material. Therefore, the natural oxide films and the almost material properties of these powders are the same. Hardness is the only property that is different in these powders. When a hard particle is deposited of on a soft substrate, the soft substrate is plastically deformed more than the hard particle. Inversely, in the case of the deposition of a soft particle on a hard substrate, the soft particle is plastically deformed more than the hard substrate. This means that the total broken area of surface oxide films on the particle and the substrate is not significantly affected by the difference in hardness. Consequently, the depositions of the milled and as-received powders are independent of each other.

As shown in Fig. 12(c), the hardness values of the coatings formed using the mixed powders fluctuate significantly; however, the hardness values of the coatings formed using either the as-received powder or the milled powder individually show limited variation. As shown in Fig. 11, the as-received powder with large crystal grains was widely distributed throughout the coating that was formed using the mixed powders. The size of the indentation

formed by the hardness test was approximately 30 μm, which is comparable with the mean diameter of the as-received powder. The areas formed by the as-received powder in the coating definitely have a lower hardness than the nanocrystalline matrix formed by the milled powder. Consequently, the hardness of the coatings formed using the mixed powders fluctuates significantly.

Based on the results, it was determined that the deposition efficiency, hardness, and porosity level of coatings formed using milled powders can be controlled by varying the content of the as-received powder of the powder mixture used for deposition. In addition, the milled and as-received powders are deposited independently from each other. This character results in a control of the microstructure of the coating. The mechanical properties of these coatings, such as their tensile strength, ductility, and adhesion strength, is aimed to be investigated in future works.

4. Conclusions

This study focused on the use of mechanical milling and cold spray techniques to develop a nanocrystalline pure iron coating. The deposition efficiency, microstructure, and hardness of each coating were assessed, and the following conclusions were drawn:

- Mechanical milling was applied to a pure iron powder with crystal grains larger than 1 μm. Consequently, nanocrystal grains of approximately 100 nm were obtained following a mechanical milling period of 20 h. In addition, it was confirmed that a wide distribution of particle sizes was obtained by the mechanical milling process.
- A dense coating consisting of nanocrystal grains could be formed by a cold spray technique using the powder that was milled for 20 h. The hardness of the coating that was formed using the milled powder was approximately double of that of the coating formed using the as-received powder. In contrast, the deposition efficiency of the coating that

was formed using the milled powder was half of that of the coating formed using the as-received powder. In addition, the porosity level of the coating formed using the milled powder was double of that of the coating formed using the as-received powder.

- The effect of the mixing ratio between the as-received and milled powders on the deposition efficiency, microstructure, hardness, and porosity level of the coating was evaluated. Nanocrystalline coatings containing randomly distributed regions consisting of coarse crystal grains were formed using the mixed powder. It was confirmed that the deposition efficiencies and porosity levels of such coatings could be controlled by varying the content of the as-received powder of the mixture used to form the coating. In addition, the milled and as-received powders are deposited on the substrate independently from each other.

Acknowledgements

This work was supported by the SUZUKI FOUNDATION. The authors are grateful to Prof. Ogawa for his support in conducting this research. The authors are grateful to Mr. Okuda for his assistance in performing the mechanical milling treatment on the powder. We would like to thank Editage (www.editage.jp) for the English language editing.

References

[1] J.R. Weertman, D. Farkas, K. Hemker, H. Kung, M. Mayo, R. Mitra, H. Van Swygenhoven, Structure and mechanical behavior of bulk nanocrystalline materials, Mater. Res. Soc. Bull. 24 (1999) 44–53. https://doi.org/10.1557/S088376940005154X

[2] C.C. Koch, D.G. Morris, K. Lu, A. Inoue, Ductility of nanostructured materials, Mater. Res. Soc. Bull. 24 (1999) 54–58. https://doi.org/10.1557/S0883769400051551

[3] Y. Wang, M. Chen, F. Zhou, E. Ma, High tensile ductility in a nanostructured metal, Nature 419 (2002) 912–914. https://doi.org/10.1038/nature01133

[4] L. Wang, J. Zhang, Y. Gao, Q. Xue, L. Hu, T. Xu, Grain size effect in corrosion behavior of electrodeposited nanocrystalline Ni coatings in alkaline solution, Scr. Mater. 55 (2006) 657–660. https://doi.org/10.1016/j.scriptamat.2006.04.009

[5] M.C. Zhao, Y.Y. Shan, The effects of thermo-mechanical control process on microstructures and mechanical properties of a commercial pipeline steel, Mater. Sci. Eng. A 335 (2002) 14–20. https://doi.org/10.1016/S0921-5093(01)01904-9

[6] Y. Iwahashi, J. Wang, Z. Horita, M. Nemoto, T.G. Langdon, Principle of equal-channel angular pressing for the processing of ultra-fine grained materials, Scr. Mater. 35 (1996) 143–146. https://doi.org/10.1016/1359-6462(96)00107-8

[7] Y. Saito, H. Utsunomiya, N. Tsuji, T. Sakai, Novel ultra-high straining process for bulk materials—development of the accumulative roll-bonding (ARB) process, Acta Mater. 47 (1999) 579–583. https://doi.org/10.1016/S1359-6454(98)00365-6

[8] C.C. Koch, Synthesis of nanostructured materials by mechanical milling: problems and opportunities, Nanostruct. Mater. 9 (1997) 13–22. https://doi.org/10.1016/S0965-9773(97)00014-7

[9] A.P. Alkhimov, S.V. Klinkov, V.F. Kosarev, A.N. Papyrin, Gas-dynamic spraying study of a plane supersonic two-phase jet, J. Appl. Mech. Tech. Phys. 38 (1997) 324–330. https://doi.org/10.1007/BF02467920

[10] A.P. Alkhimov, V.F. Kosarev, A.N. Papyrin, Gas-dynamic spraying. An experimental study of the spraying process, J. Appl. Mech. Tech. Phys. 39 (1998) 318–323. https://doi.org/10.1007/BF02468100

[11] J. Liu, X. Zhou, X. Zheng, H. Cui, J. Zhang, Tribological behavior of cold-sprayed nanocrystalline and conventional copper coatings, Appl. Surf. Sci. 258 (2012) 7490–7496. https://doi.org/10.1007/s11249-016-0646-2

[12] Q. Zhang, Chang-Jiu Li, Cheng-Xin Li, Guan-JunYang, Siu-Ching Lui, Study of oxidation behavior of nanostructured NiCrAlY bond coatings deposited by cold spraying, Surf. Coat. Tech. 202 (2008) 3378–3384. https://doi.org/10.1016/j.surfcoat.2007.12.028

[13] N. Kaura, M. Kumar, Sanjeev K. Sharma, D.Y. Kim, S. Kumar, N.M. Chavan, S.V. Joshi, N. Singh, H. Singh, Study of mechanical properties and high temperature oxidation behavior of a novel cold-spray Ni-20Cr coating on boiler steels, Appl. Surf. Sci. 328 (2015) 13–25. https://doi.org/10.1016/j.apsusc.2014.12.033

[14] H. Wang, C. Li, G. Yang, C. Li, Q. Zhang, W. Li, Microstructural characterization of cold-sprayed nanostructured FeAl intermetallic compound coating and its ball-milled feedstock powders, J. Therm. Spray Technol. 16 (2007) 669–676.

[15] A.C. Hall, L.N. Brewer, T.J. Roemer, Preparation of aluminum coatings containing homogenous nanocrystalline microstructures using the cold spray process, J. Therm. Spray Technol. 17 (2008) 352–359. https://doi.org/10.1007/s11666-007-9089-5

[16] Y.Y. Zhang, X.K. Wu, H. Cui, J.S. Zhang, Cold-spray processing of a high density nanocrystalline aluminum alloy 2009 coating using a mixture of as-atomized and as-cryomilled powders, J. Therm. Spray Technol. 20 (2011) 1125–1132. https://doi.org/10.1007/s11666-011-9652-y

[17] L. Ajdelsztajn, J.M. Schoenung, B. Jodoin, G.E. Kim, Cold spray deposition of nanocrystalline aluminum alloys, Metall. Mater. Trans. A 36 (2005) 657–666. https://doi.org/10.1007/s11661-005-0182-4

[18] M. Kumar, H. Singh, N. Singh, Sung-Min Hong, In-Suk Choi, Jin-Yoo Suh, N.M. Chavan, S. Kumar, S.V. Joshi, Development of nano-crystalline cold sprayed Ni–20Cr coatings for high temperature oxidation resistance, Surf. Coat. Tech. 266 (2015) 122–133. https://doi.org/10.1016/j.surfcoat.2015.02.032

[19] M. Kumar, H. Singh, N. Singh, Sung-Min Hong, In-Suk Choi, Jin-Yoo Suh, N.M. Chavan, S. Kumar, S.V. Joshi, Erosion–corrosion behavior of cold-spray nanostructured Ni–20Cr coatings in actual boiler environment, Wear 332-333 (2015) 1035–1043. https://doi.org/10.1016/j.wear.2015.01.043

[20] C.A. Schneider, W.S. Rasband, K.W. Eliceiri, NIH Image to ImageJ: 25 years of image analysis, Nature Methods 9 (2012) 671–675. http://doi.org/10.1038/nmeth.2089

[21] B. Al-Mangour, P. Vo, R. Mongrain, E. Irissou, S. Yue, Effect of heat treatment on the microstructure and mechanical properties of stainless steel 316L coatings produced by cold spray for biomedical applications, J. Therm. Spray Technol. 23 (2014) 641–652. https://doi.org/10.1007/s11666-013-0053-2

[22] K. Ito, Y. Ichikawa, K. Ogawa, Experimental and numerical analyses on the deposition behavior of spherical aluminum particles in the cold-spray-emulated high-velocity impact process, Mater. Trans. 57 (2016) 525–532. https://doi.org/10.2320/matertrans.T-M2016803

[23] T. Schmidt, H. Assadi, F. Gärtner, H. Richter, T. Stoltenhoff, H. Kreye, T. Klassen, From particle acceleration to impact and bonding in cold spraying, J. Therm. Spray Technol. 18 (2009) 794–808. https://doi.org/10.1007/s11666-009-9357-7

[24] B. Jodoin, L. Ajdelsztajn, E. Sansoucy, A. Zúñiga, P. Richer, E.J. Lavernia, Effect of particle size, morphology, and hardness on cold gas dynamic sprayed aluminum alloy coatings, Surf. Coat. Tech. 201 (2006) 3422–3429. https://doi.org/10.1016/j.surfcoat.2006.07.232

[25] Z. Zhang, S. K. Vajpai, D. Orlov, K. Ameyama, Improvement of mechanical properties in SUS304L steel through the control of bimodal microstructure characteristics, Mater. Sci. Eng. A 598 (2014) 106–113. https://doi.org/10.1016/j.msea.2014.01.023

[26] K. Ogawa, K. Ito, Y. Ichikawa, S. Ohno, N. Onda, Characterization of low-pressure cold-sprayed aluminum coatings, J. Therm. Spray Technol. 17 (2008) 728–735. https://doi.org/10.1007/s11666-008-9254-5

Table I Chemical composition of the pure iron powder [unit: wt.%].

C	Si	Mn	P	S	Fe
0.007	0.01	0.06	0.015	0.006	Bal.

List of figure captions

Figure 1 SEM images of the as-received powder and the powders that were mechanically milled for various treatment periods; (a) as-received, (b) milled for 5 h, (c) milled for 10 h, and (d) milled for 20 h.

Figure 2 Particle-size distribution of the as-received powder and the powders that were milled for various periods.

Figure 3 Relationship between the mean particle size and the mechanical milling treatment period.

Figure 4 IPF images obtained from the cross-section of each powder; (a) as-received powder, (b) powder milled for 20 h (low magnification), (c) powder milled for 20 h (high magnification).

Figure 5 Crystal grain-size distribution of the as-received powder and the powder that was mechanically milled for 20 h.

Figure 6 Cross-sectional SEM images of each coating; (a) STD specimen, (b) magnified STD specimen, (c) MM specimen, and (d) magnified MM specimen.

Figure 7 IPF image obtained from the cross-section of each coating; (a) STD specimen, (b) STD specimen, (c) MM specimen, and (d) magnified MM specimen.

Figure 8 Crystal grain-size distribution of the STD specimen and the MM specimen.

Figure 9 Hardness, deposition efficiency, and porosity level of the STD and the MM specimens; (a) hardness, (b) deposition efficiency, and (c) porosity.

Figure 10 Cross-sectional SEM image of the coatings formed using each mixed powder; (a) AS10 coating, (b) magnified AS10 coating, (c) AS20 coating, (d) magnified AS20 coating, (e) AS30 coating, and (f) magnified AS30 coating.

Figure 11 IPF image obtained from the cross-section of each coating; (a) AS10 coating, (b) AS20 coating, and (c) AS30 coating.

Figure 12 Dependency of deposition efficiency, porosity level, and hardness on the content of the as-received powder of the mixture used to form the coating; (a) deposition efficiency, (b) porosity, and (c) hardness.

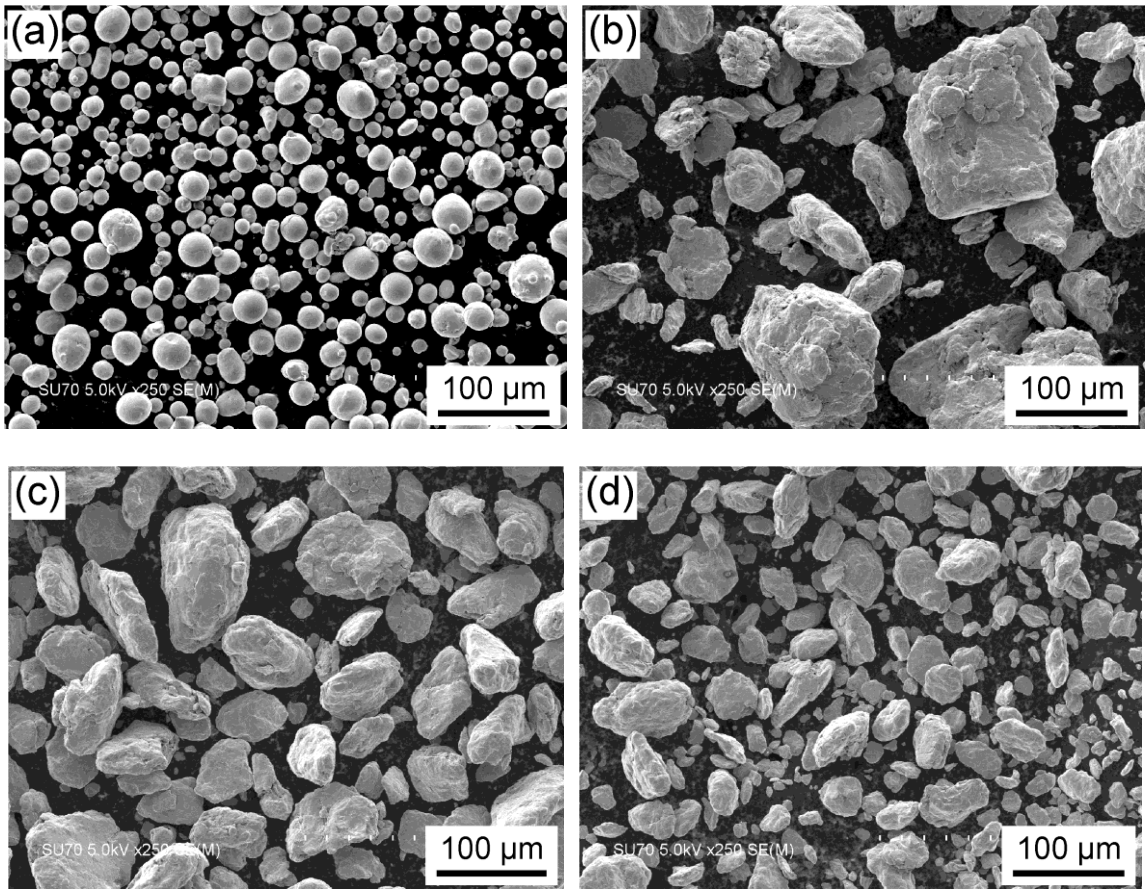
(a)
100 μm
(b)
SU70 5.0kV x250 SE(M)
100 μm
(c)
100 μm
(d)
SU70 5.0kV x250 SE(M)
100 μm

Figure 1

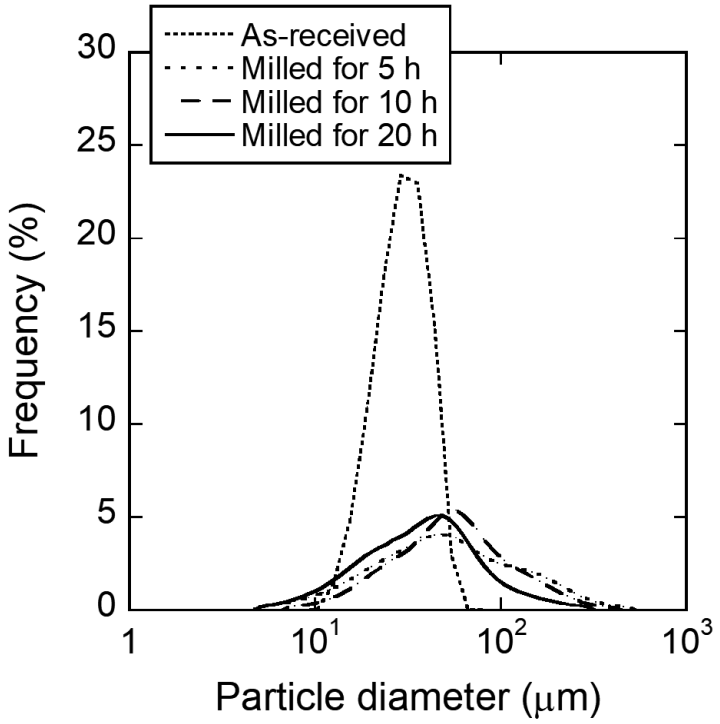
As-received
Milled for 5 h
Milled for 10 h
Milled for 20 h
Frequency (%)
Particle diameter (μm)
0
5
10
15
20
25
30
1
10^1
10^2
10^3

Figure 2

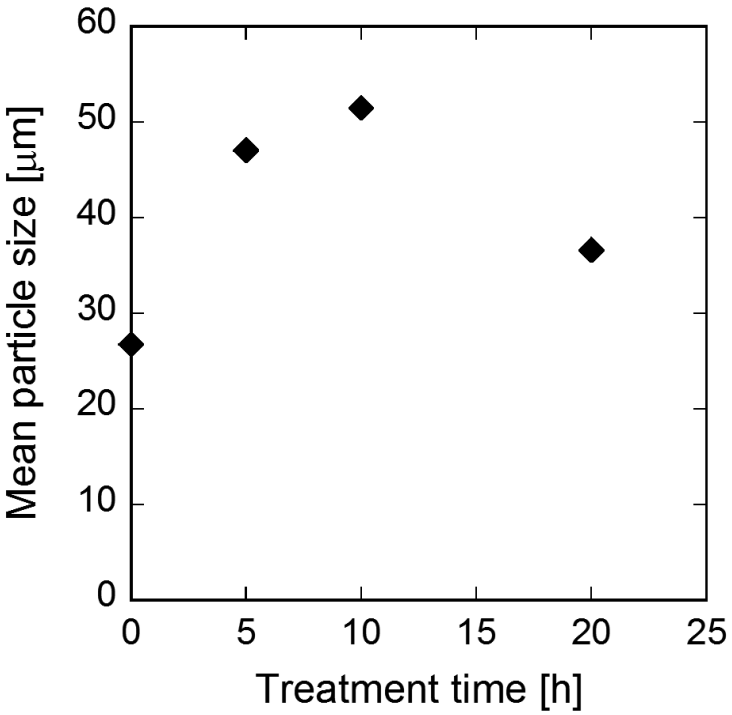
Mean particle size [μm]
60
50
40
30
20
10
0
0
5
10
15
20
25
Treatment time [h]

Figure 3

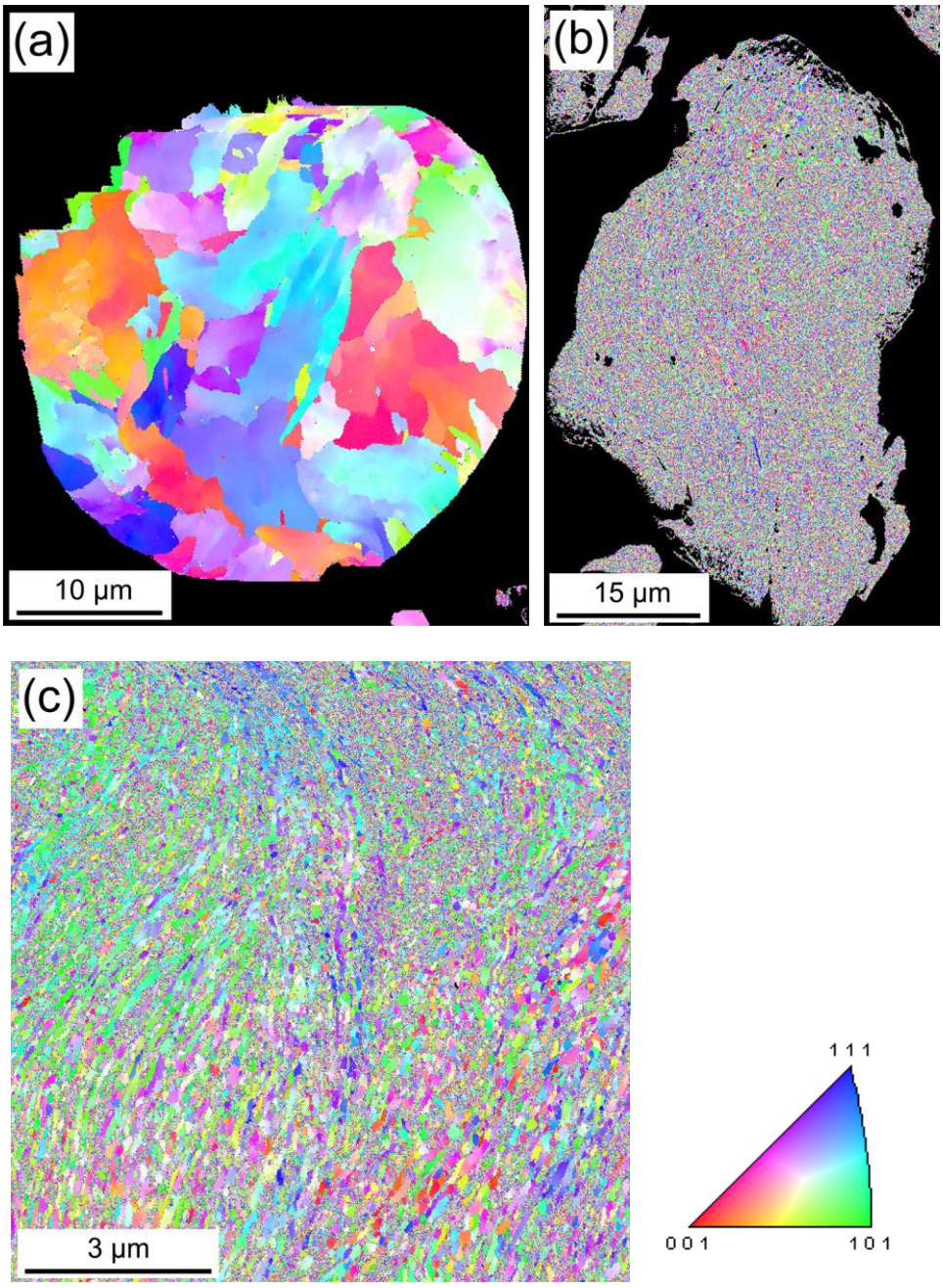

Figure 4

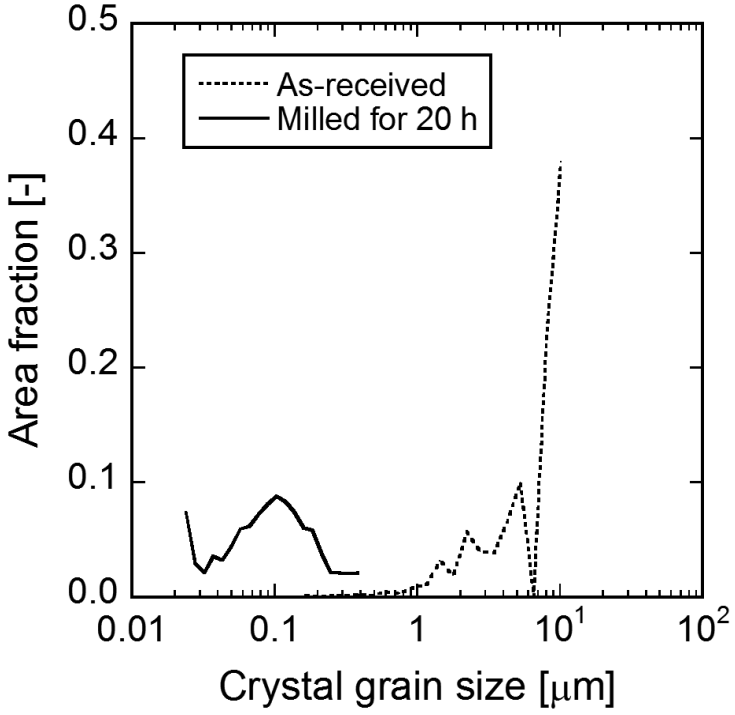
0.5
0.4
0.3
0.2
0.1
0.0
Area fraction [-]
As-received
Milled for 20 h
0.01
0.1
1
10^1
10^2
Crystal grain size [μm]

Figure 5

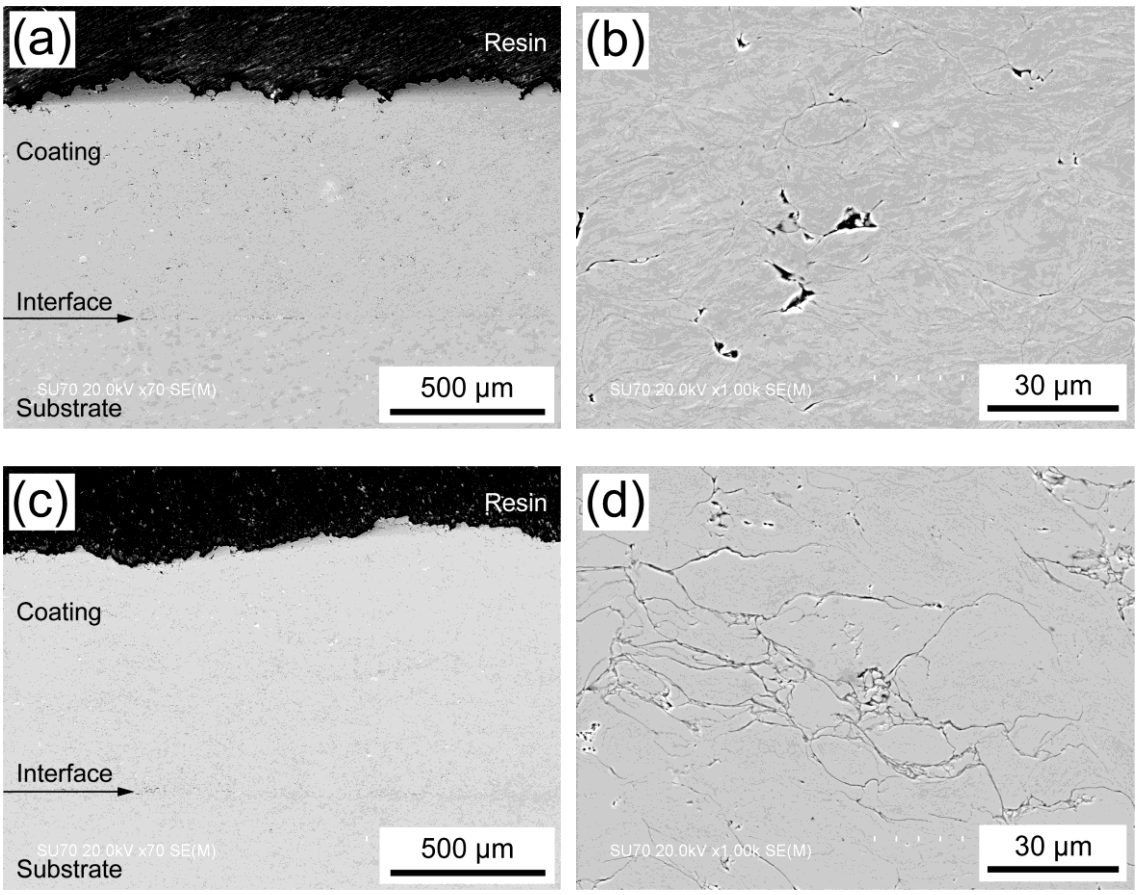
(a)
Resin
Coating
Interface
SU70 20.0kV x70 SE(M)
500 μm
Substrate
(b)
SU70 20.0kV x1.00k SE(M)
30 μm
(c)
Resin
Coating
Interface
SU70 20.0kV x70 SE(M)
500 μm
Substrate
(d)
SU70 20.0kV x1.00k SE(M)
30 μm

Figure 6

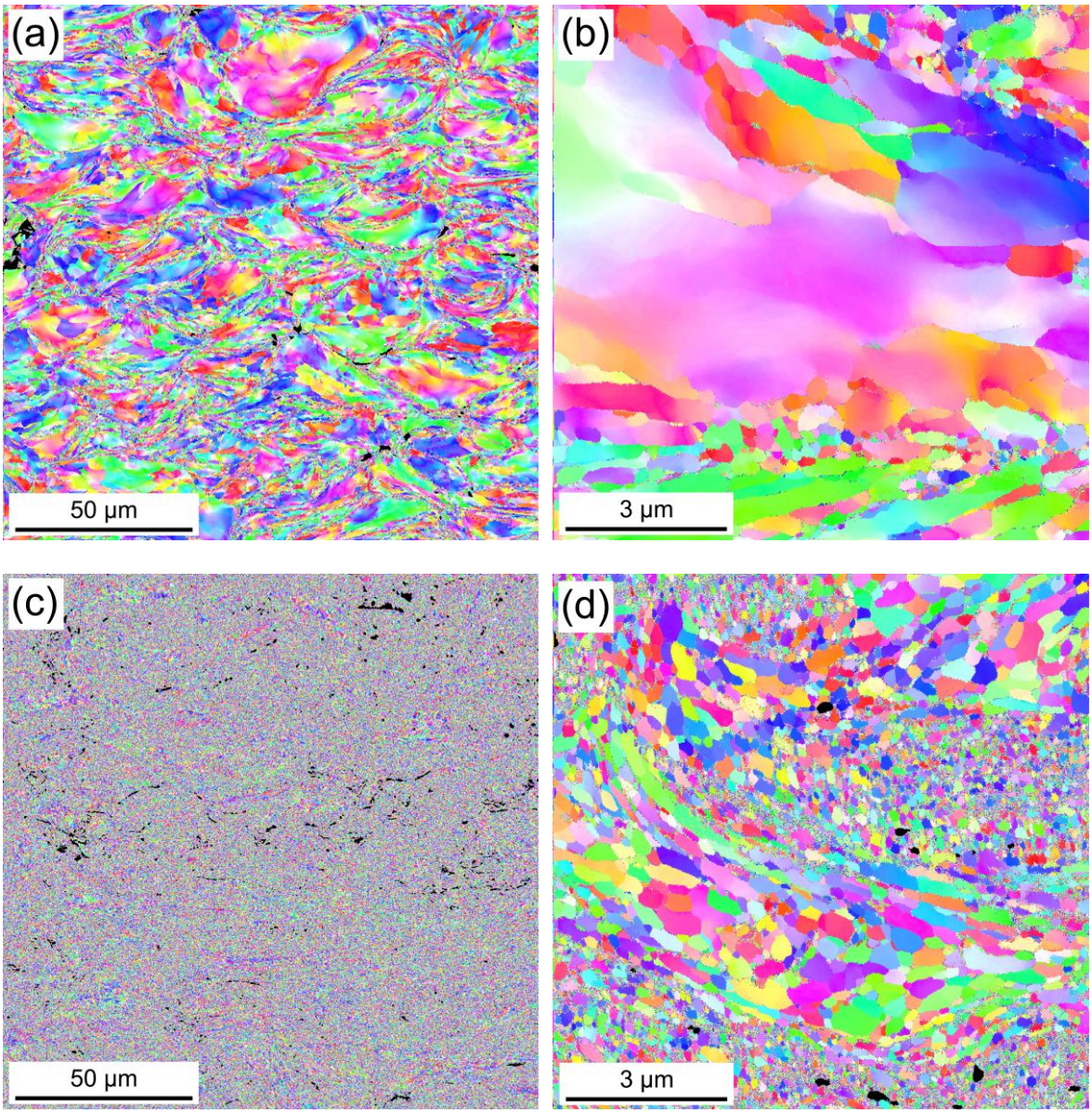

Figure 7

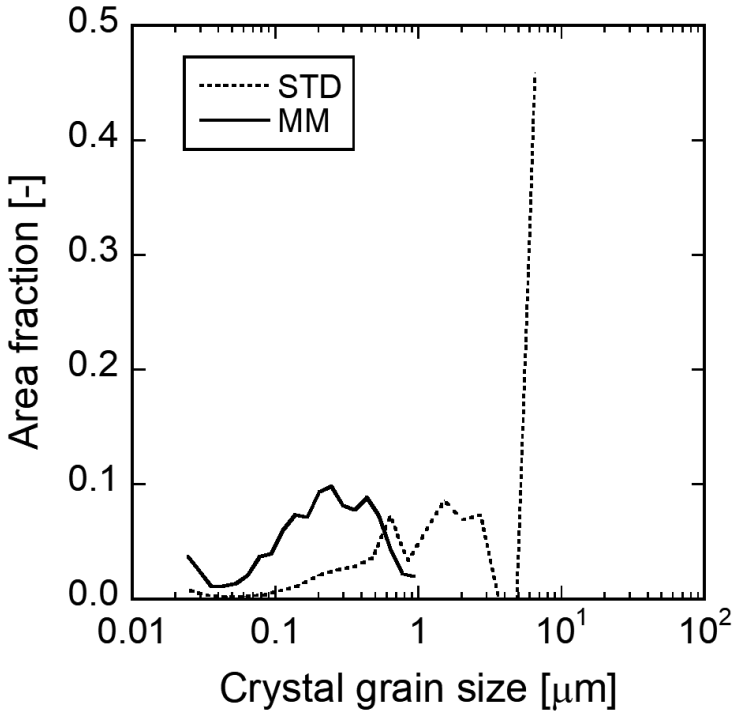
0.5
0.4
0.3
0.2
0.1
0.0
Area fraction [-]
STD
MM
0.01
0.1
1
10^1
10^2
Crystal grain size [μm]

Figure 8

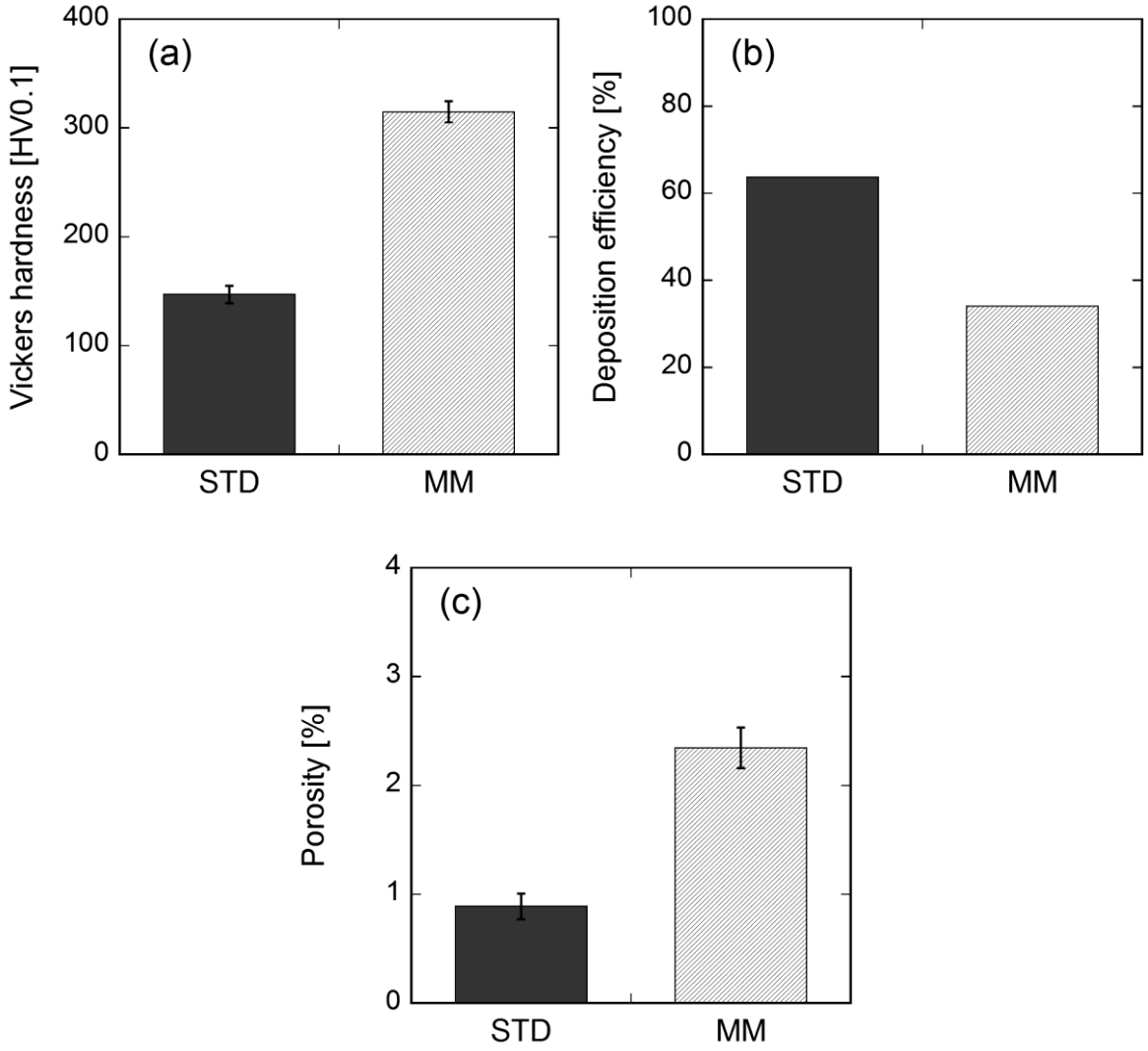
(a)
Vickers hardness [HV0.1]
400
300
200
100
0
STD
MM
(b)
Deposition efficiency [%]
100
80
60
40
20
0
STD
MM
(c)
Porosity [%]
4
3
2
1
0
STD
MM

Figure 9

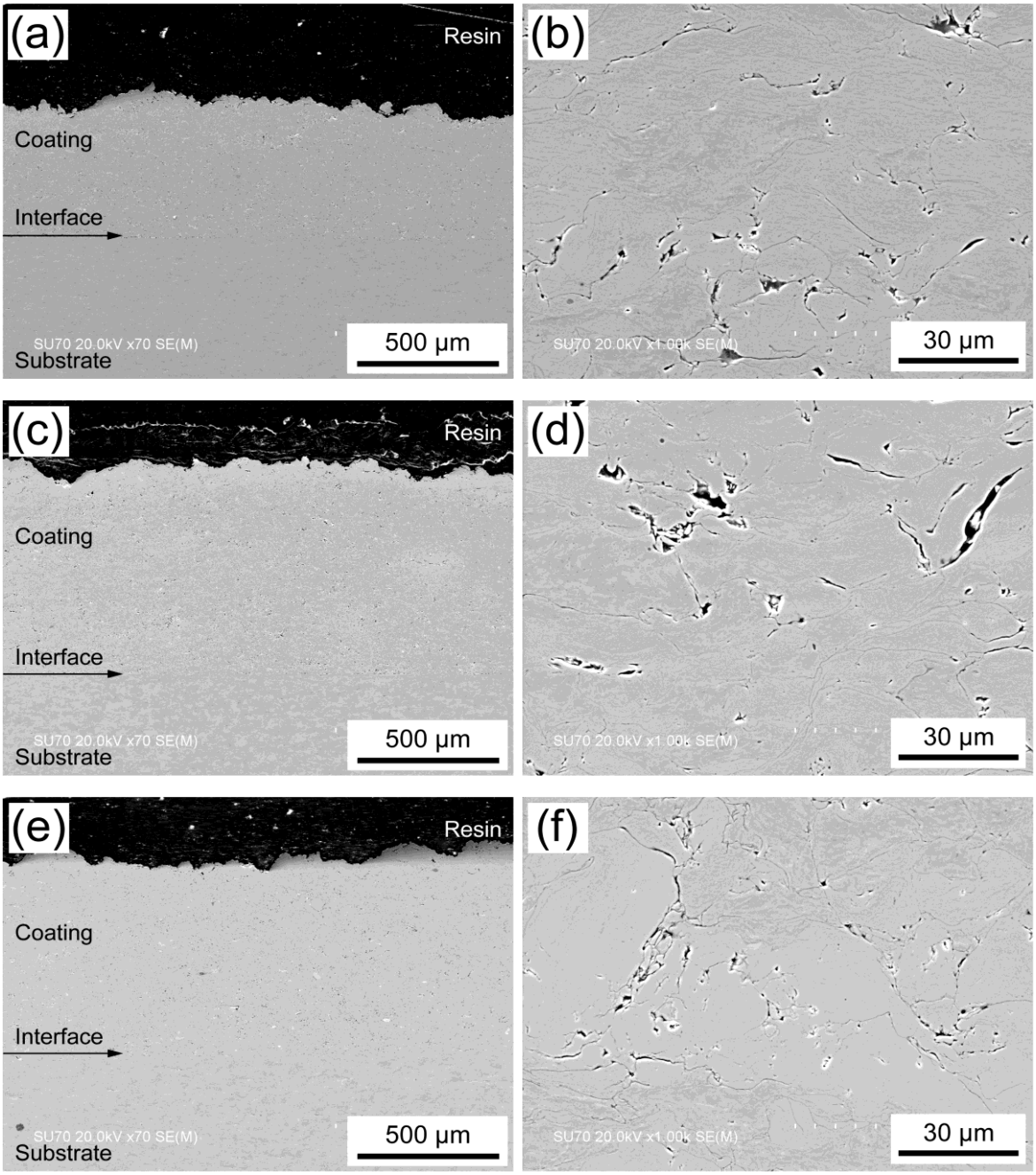
(a)
Resin
Coating
Interface
SU70 20.0kV x70 SE(M)
500 μm
Substrate
(b)
SU70 20.0kV x1.00k SE(M)
30 μm
(c)
Resin
Coating
Interface
SU70 20.0kV x70 SE(M)
500 μm
Substrate
(d)
SU70 20.0kV x1.00k SE(M)
30 μm
(e)
Resin
Coating
Interface
SU70 20.0kV x70 SE(M)
500 μm
Substrate
(f)
SU70 20.0kV x1.00k SE(M)
30 μm

Figure 10

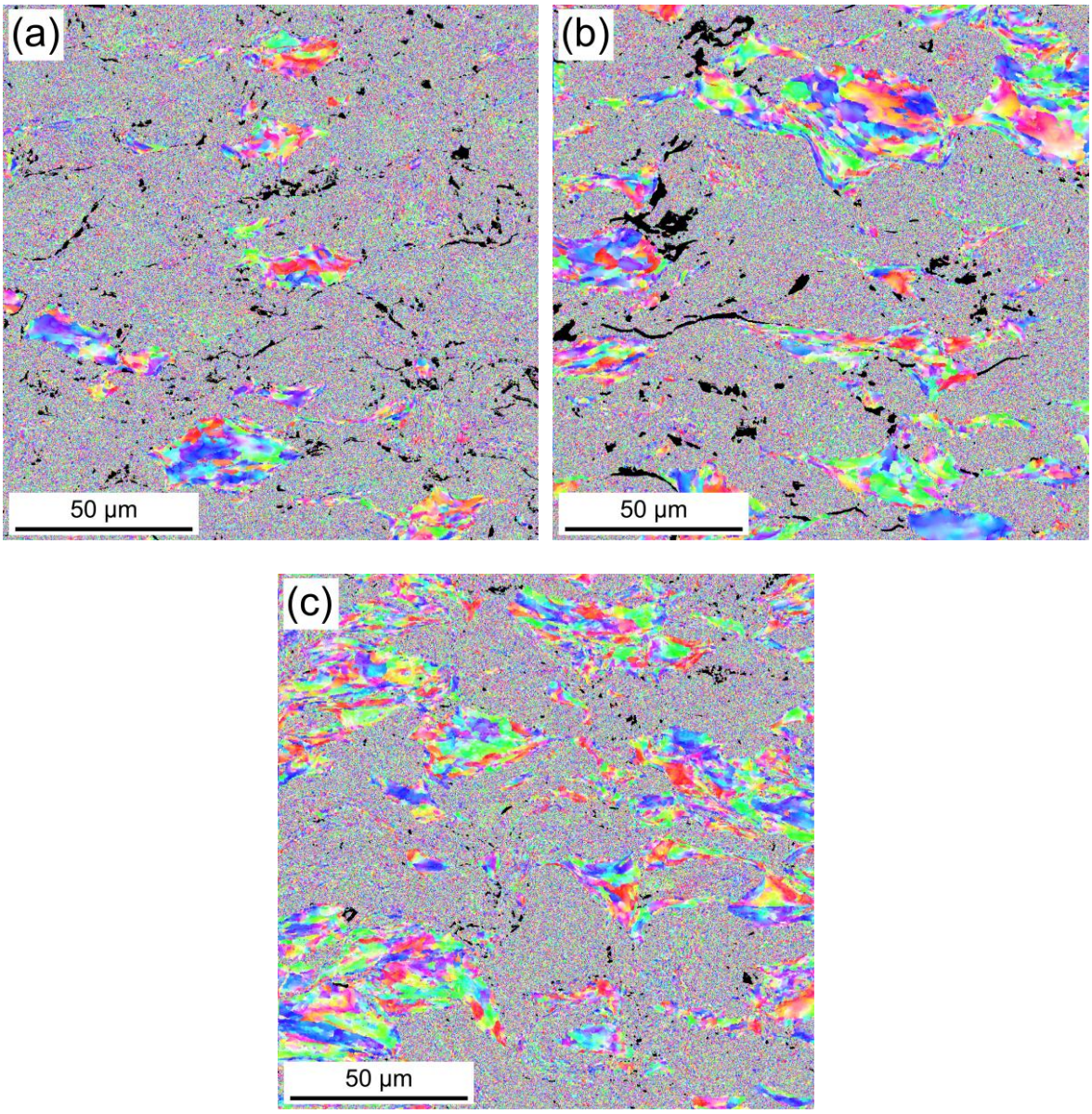

Figure 11

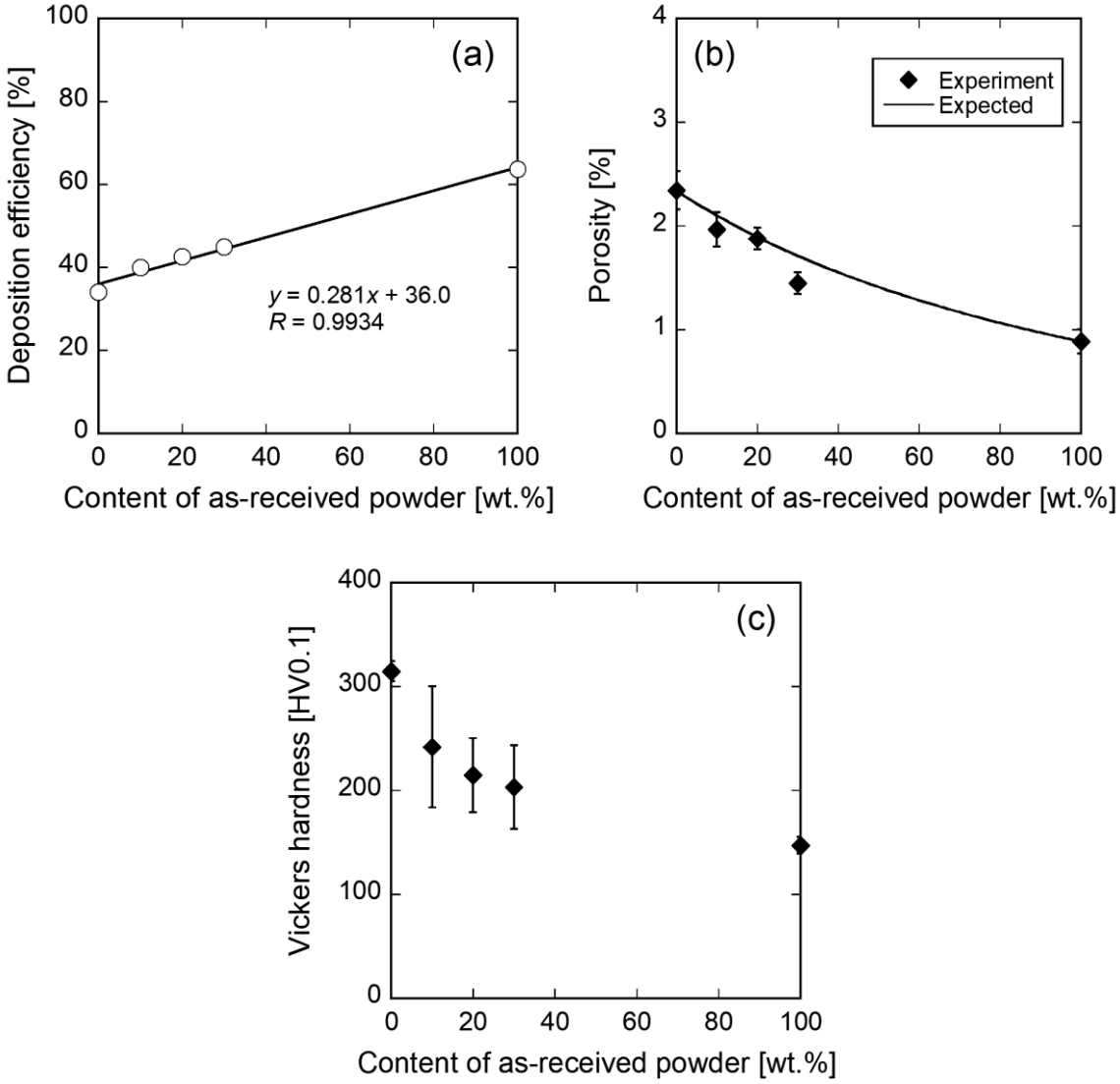
(a)
Deposition efficiency [%]
Content of as-received powder [wt.%]
y = 0.281x + 36.0
R = 0.9934
(b)
Porosity [%]
Experiment
Expected
Content of as-received powder [wt.%]
(c)
Vickers hardness [HV0.1]
Content of as-received powder [wt.%]

Figure 12